

Electrical Properties of Staggered Electrode, Solution-Processed, Polycrystalline Tetrabenzoporphyrin Field-Effect Transistors

Patrick B. Shea, *Student Member, IEEE*, Aaron R. Johnson, Noboru Ono, and Jerzy Kanicki, *Senior Member, IEEE*

Abstract—We characterize and analyze the electrical performance of solution-processed, polycrystalline tetrabenzoporphyrin thin-film field-effect transistors with staggered source and drain contacts. Devices demonstrated a saturation field-effect mobility and threshold voltage on the order of 10^{-2} cm²/V-s and -15 V, respectively, as well as a subthreshold slope of 1.2 V/decade and an ON/OFF-current ratio exceeding 10^5 . The device performance and electronic properties of the thin film were used to construct device energy band diagrams. Lastly, the device conduction mechanism is discussed.

Index Terms—Absorbance, cyclic voltammetry, organic field-effect transistors (OFETs), porphyrins, solution processing, staggered electrodes.

I. INTRODUCTION

SOLUTION processable organic small molecule semiconductors have proven viable materials for the channel region of organic thin-film field-effect transistors (OFETs) [1]–[6]. Thin films of organic small molecules, such as pentacene or copper phthalocyanine, have traditionally been formed using high vacuum evaporation [7]. However, such a method precludes cost effective, large area, high volume device fabrication. By utilizing precursor forms of the organic small molecules, however, the adaptive and cost effective nature of solution processing is available [8]. A particular class of organic small molecules, porphyrins, has demonstrated solution processable OFET performance on par with their evaporated antecedents [4], [6] [9]. While the coplanar, or bottom-contact, source and drain (S/D) structure allows for fabrication of devices en masse, it can introduce contact quality problems due to poor step coverage over the S/D electrodes, or poor adhesion of the metal to the insulator or the organic semiconductor to the electrodes; poor step coverage in turn introduces morphological discontinuities of the organic semiconductor near the metal electrodes. Staggered, or top-contact, S/D electrodes can avoid these problems that introduce high contact resistance; combined with solution processable porphyrins that become nearly impervious to organic solvents or high temperature processing [6], they are potentially robust, high-performance

structures. Yet this configuration is not often discussed in detail for small molecules [5], [10]; several works exist discussing their effects on polymer-based devices [11]–[13]. Furthermore, due to the great interest in the commercial development of organic semiconductor technologies, many researchers have examined charge injection between electrodes (either metal or otherwise) and organic semiconductors [14]–[17]. Indeed, the development of novel, solution-processable organic small molecule semiconductors may induce study of these materials more in the likeness of amorphous or polycrystalline silicon thin-film transistors [18], [19]. This work provides analysis on the electrical performance of staggered S/D electrodes in solution-processed polycrystalline tetrabenzoporphyrin OFETs.

II. EXPERIMENTAL

The staggered OFET structures used in this study were fabricated on n++ (0.008–0.02 Ω-cm) crystalline Si (c-Si) wafers coated with a 100-nm thermal oxide. The heavily-doped c-Si substrate is used as an unpatterned gate electrode. The thermal oxide dielectric, with a measured capacitance per unit area $C_i = 24.5$ nF/cm², served as the gate insulator and was cleaned by washing in acetone and isopropyl alcohol, followed by a 20-min exposure to UV/ozone and a 20-min soak in 200-proof ethanol. After drying the cleaned substrate in N₂ gas, 1, 4:8, 11:15, 18–22, 25-tetraethano-29H, 31H-tetrabenzoporphyrin (CP) (0.7% weight in chloroform) was spun-cast onto the thermal oxide at 1000 rpm for 30 s. The CP film was then converted to tetrabenzoporphyrin (29H, 31H-tetrabenzoporphyrin, or TBP) by heating at 210 °C for 5 min, such that volatile C₂H₄ side chains are removed, thus transforming the film from amorphous and soluble, to polycrystalline and insoluble [6]; the final film thickness was measured to be 120 nm. Source and drain electrodes were then formed on top of the converted film by slow thermal evaporation of 40 nm of gold in high vacuum (<0.3 Å/s at $\sim 10^{-6}$ Torr) through a stencil mask. Electrical contact to the n++ c-Si backside was made with indium gallium eutectic. The source electrode was biased as common for all measurements. To operate in accumulation mode and inject electrons at the drain, the gate and drain electrodes were biased negative in relation to a common source electrode. Transfer characteristics (drain current—gate-to-source voltage, or $I_D - V_{GS}$) were measured from the ON-state, when the gate-to-source bias is more negative than the OFET threshold voltage, V_T , ($V_{GS} < V_T$) to the OFF-state ($V_{GS} > V_T$), when the gate-to-source bias is more positive than the threshold

Manuscript received December 28, 2004. The review of this paper was arranged by Editor S. Datta.

The authors are with the Department of Electrical Engineering and Computer Science, The University of Michigan, Ann Arbor, MI 48109 USA (e-mail: kanicki@eecs.umich.edu).

N. Ono is with the Department of Chemistry, Faculty of Science, Ehime University, Matsuyama 790-8577, Japan.

Digital Object Identifier 10.1109/TED.2005.850616

voltage. Output characteristics ($I_D - V_{DS}$) were measured from low V_{DS} to high V_{DS} , where V_{DS} is the drain-to-source bias. Measurements were performed in air and in the dark. The results presented herein are for an interdigitated structure with a channel length $L = 22.5 \mu\text{m}$, and channel width consisting of 20 digits, each of width $W' = 600 \mu\text{m}$, for a total channel width $W = 12 \text{ mm}$. Several device geometries, with varying channel widths and lengths, were tested and corroborate the presented data in relation to their ohmic-like behavior.

For optical absorbance measurements, glass substrates were cleaned and coated using the aforementioned process; a second, uncoated glass substrate was also cleaned and scanned for reference. Absorbance versus wavelength was measured in air at room temperature using a Varian-Cary 5e UV-visible spectrometer and normalized to the maximum absorbance over a range of $200 \leq \lambda(\text{nm}) \leq 1500$.

The CH Instruments 660a cyclic voltammetry measurement system consisted of a three-electrode, undivided cell filled with a solution of 0.1 M tetra-n-butylammonium hexafluorophosphate (TBAPF6) in acetonitrile. The three electrodes used for measurement consist of one glassy carbon working electrode coated with the thin film of interest, one reference electrode containing 0.1 M TBAPF6 and 0.01 M AgNO_3 in acetonitrile, and one platinum counter electrode. The working electrode was prepared by dip-coating in a solution of CP, followed by annealing of CP to TBP. High-temperature processing did not produce noticeable problems with the operation of the working electrode. Excess water was driven from the TBAPF6 solution before testing by bubbling N_2 through the solution. Two TBP-coated working electrodes were produced and scanned from 0 to 2 V and 0 to -3 V , respectively, at a rate a 0.1 V/s. The resulting current was measured and analyzed as a function of voltage (V), with peaks in the current (C) indicating oxidation (positive voltage) and reduction (negative voltage) processes. To convert voltage measurements to a comparable energy scale, ferrocene was introduced into the solution and scanned using a third, blank working electrode. The energy level of ferrocene is known [20], and provides a reference to convert the electrode voltage in volts to an energy in eV related to the vacuum level. The film ionization potential and electron affinity were calculated by subtracting the baseline solution effect (the dashed lines in Fig. 4) from the CV spectrum and by approximating the slope of the current peak with a straight line (the dotted lines in Fig. 4). This simple method allows determination of the reduction and oxidation voltages by the intersection of the baseline and the linear approximation.

III. OFET ELECTRICAL PERFORMANCE

Output characteristics shown in Fig. 1(a) indicate that transistor action is achieved in the staggered-electrode TBP OFETs, and displays distinct linear and saturation operating regimes. Near the origin, little onset delay in I_D occurs as the drain bias is increased, with the onset delay being defined as points where $I_D > 0$. The linear regime characteristics exhibit minimal bowing or superlinear behavior; in the saturation regime

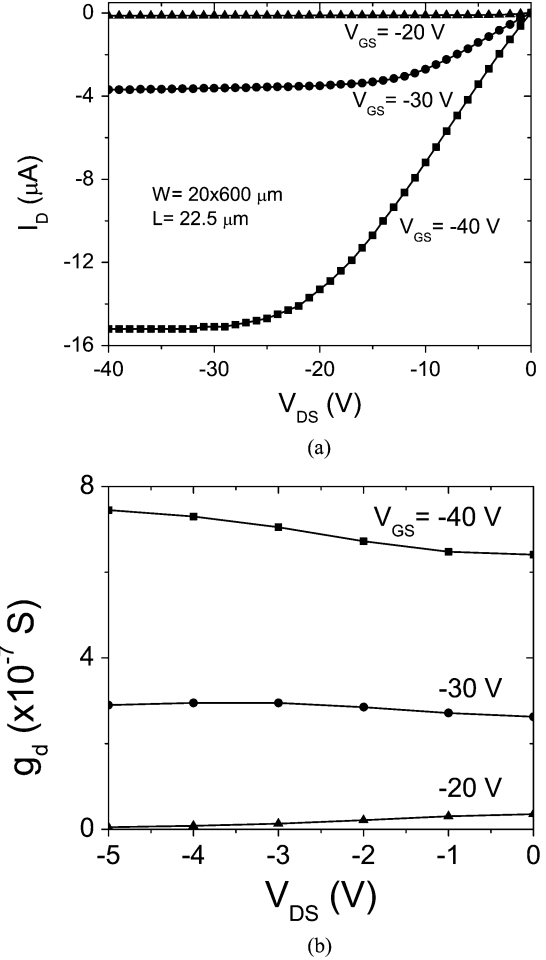


Fig. 1. (a) Output characteristics and (b) conductance g_d of the staggered Au S/D TBP OFETs.

the drain current remains nearly constant above $V_{DS} < V_{GS} - V_T$. However, a differential examination of the conductance

$$g_d = \frac{dI_D}{dV_{DS}} = \frac{W}{L} \mu_{FE} C_i [(V'_{GS} - V_T) - V'_{DS}] \quad (1)$$

at low drain bias reveals a nonmonotonic behavior in the differential current. Such g_d behavior is typically indicative of current crowding, as well as high or nonlinear contact resistance effects [21]. In this case, g_d increases slightly, then declines at higher drain biases, indicating that at low drain bias the current increases at a rate faster than predicted by the linear regime metal-oxide-semiconductor field-effect transistors (MOSFETs) drain current equation [21]. The gradual channel approximation of the drain current for c-Si p-channel MOSFET, which assumes a long transistor channel over which the electric-field accumulating carriers at the channel is greater than the electric field from drain to source, was used to derive the current-voltage relations given here, including a correction for contact resistance [22]

$$I_D = -\frac{W}{L} \mu_{FE} C_i [(V'_{GS} - V_T) - V'_{DS}/2] V'_{DS} \quad (2)$$

where μ_{FE} is the field-effect mobility, V_T is the threshold voltage, C_i is the areal gate capacitance, R_C is the sum of the drain and source contact resistances, $V'_{DS} = V_{DS} - 2R_C I_D$,

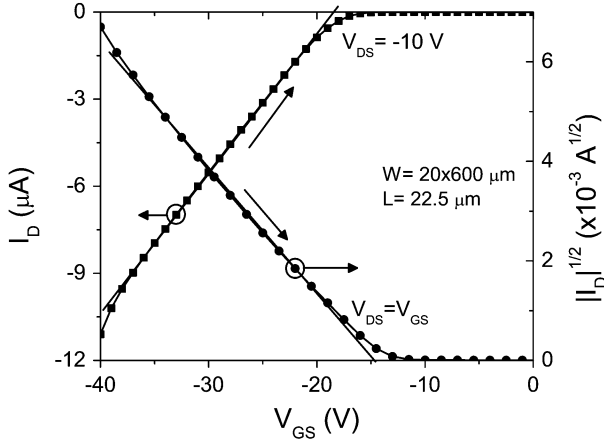


Fig. 2. Linear-scale transfer characteristics used for extraction of μ_{FE} and V_T of the staggered Au S/D contact TBP OFET. Arrows indicate the measurement direction.

and $V'_{GS} = V_{GS} - R_C I_D$. In the linear regime when $|V'_{DS}| \ll |V'_{GS} - V_T|$, (2) simplifies to

$$I_D^{Lin} = -\frac{W}{L} \mu_{FE}^{Lin} C_i (V'_{GS} - V_T^{Lin}) V'_{DS} \quad (3)$$

and in the saturation regime

$$I_D^{Sat} = -\frac{W}{2L} \mu_{FE}^{Sat} C_i (V'_{GS} - V_T^{Sat})^2. \quad (4)$$

Although the previous equations, which were derived for MOSFETs, are commonly used to analyze OFETs, we must recognize that their usefulness in characterizing such devices breaks down when one considers the inherent differences between MOSFET and OFETs [23]–[25]. The threshold voltage in a MOSFET is a calculable value based on the semiconductor, its doping levels, and other predetermined fabrication processes, and for an inverted p-channel device can be described by [21]

$$V_T = V_{FB} - 2|\Psi_b| - \frac{\sqrt{4q\epsilon_{semi}N_D^+|\Psi_b|}}{C_{ins}} \quad (5)$$

where V_{FB} is the flatband energy voltage, Ψ_B is the difference between the Fermi level and the intrinsic Fermi level, q is the Coulombic charge of 1.602×10^{-19} C, ϵ_{semi} is the permittivity of the semiconductor, N_D^+ is the ionized donor concentration, and C_{ins} is the aerial gate capacitance. Since V_T in OFETs is related to trap state densities in the thin film, (5) needs to be modified [24]. Furthermore, the transfer characteristics for even long-channel OFETs often display significant nonlinearity, indicating a gate- and drain-bias dependent field-effect mobility [22], [23], [25]. In the first-order approximation for OFETs, V_T and μ_{FE} are extracted from the transfer characteristics (Fig. 2) using a linear best-fit model of I_D from (3) and $\sqrt{|I_D|}$ from (4); V_T is determined to be the x-axis intercept and indicates the gate voltage at which significant charge carrier conduction occurs between the source and drain terminals, while μ_{FE} is determined by the slope of this best-fit line. The methodology used here for extracting the device performance parameters has been applied previously to hydrogenated amorphous Si (a-Si:H)

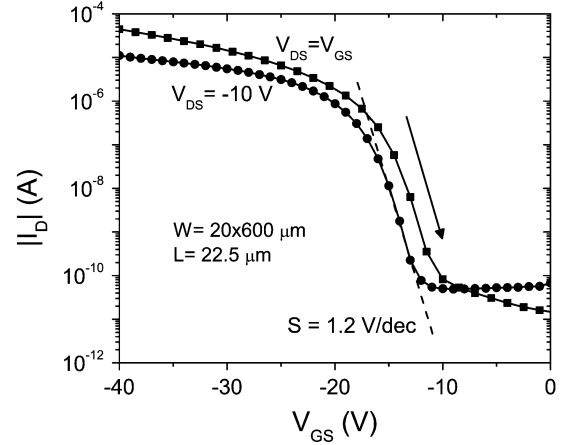


Fig. 3. Semilogarithmic transfer characteristics of the staggered Au S/D contact TBP OFET. The arrow indicates the measurement direction, and the dashed line represents the gate bias region where the subthreshold slope was determined.

thin-film transistors (TFTs) and OFETs, and is outlined in several comprehensive works [19], [25]–[27].

Our results indicate that the field-effect mobility and threshold voltage of staggered electrode TBP OFETs, for the channel-length scale examined ($\geq 15 \mu\text{m}$), are independent of channel length, from $15 \mu\text{m}$ to $100 \mu\text{m}$. Extraction of V_T^{Lin} and μ_{FE}^{Lin} from I_D in the linear regime with $V_{DS} = -10$ V yields $V_T^{Lin} = -18.4$ V and $\mu_{FE}^{Lin} = 3.6 \times 10^{-3} \text{ cm}^2/\text{V}\cdot\text{s}$. Furthermore, the ON/OFF-current ratio was determined from the semilogarithmic plot of I_D (Fig. 3) between $V_{GS} = -40$ V and -10 V to be approximately $10^{-5}/10^{-10} \approx 10^5$. The accumulation subthreshold slope is calculated by [28]

$$S = \frac{kT}{q \log(e)} \times [1 + C_i (\sqrt{\epsilon_s N_{bs}} + q N_{ss})]. \quad (6)$$

We speculate that the subthreshold behavior is dominated by the trap states in the grain boundary regions of the polycrystalline thin film [29], and have reported a maximum surface trap states density of $N_{ss}^{max} = 2.9 \times 10^{12} \text{ cm}^{-2}\cdot\text{eV}^{-1}$ and a bulk trap states density of $N_{bs}^{max} = 4.10 \times 10^{18} \text{ cm}^{-3}\cdot\text{eV}^{-1}$ [9].

Saturation regime extraction of V_T^{Sat} and μ_{FE}^{Sat} from I_D with $V_{DS} = V_{GS}$ yields $V_T^{Sat} = -14.7$ V and $\mu_{FE}^{Sat} = 9.9 \times 10^{-3} \text{ cm}^2/\text{V}\cdot\text{s}$. The extracted V_T^{Sat} and μ_{FE}^{Sat} differ from the linear regime values due to the square-law quadratic dependence of I_D^{Sat} on V_{GS} in the ideal MOSFET equations, given the graphical method by which they are calculated, and the gate-dependent mobility which produces a nonlinear transfer characteristic [23], [25]–[27]. It is worth noting here that, as previously shown [9], the transfer characteristics of the TBP OFETs described here are highly linear with respect to OFETs made using other organic semiconductors [30], and provide a good fit to the gradual channel approximation. Additionally, the gate leakage current was negligible at varied V_{GS} .

IV. OPTICAL AND ELECTRONIC PROPERTIES OF TETRABENZOPORPHYRIN

By studying the electronic and optical properties of TBP thin films, we can provide a more complete picture into the electrical

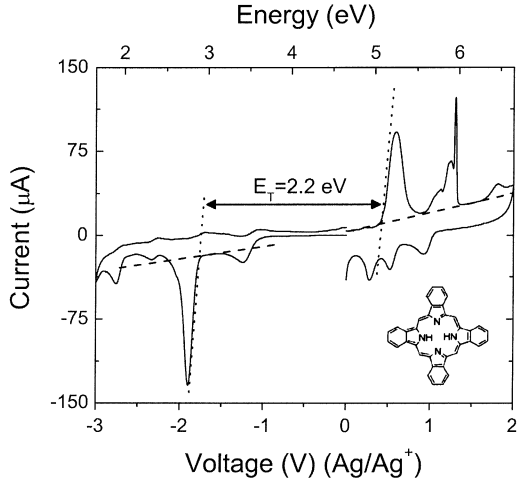


Fig. 4. Cyclic voltammogram for a TBP thin film.

operation of TBP OFETs in conjunction with their electronic structure. One useful electrochemical method for studying the electronic structure of a thin film is cyclic voltammetry [31], [32], wherein applying a voltage to an electrochemical cell yields a cyclic voltammogram revealing the oxidation and reduction properties of a thin film in the electrochemical cell. Voltages where a thin film oxidizes and reduces are indicated by increases in the electrode current, and can be used to study occupied and unoccupied molecular orbital energy levels, and thereby construct an approximate energy bandstructure. This is based on the assumption that the reduction and oxidation potentials correspond to the ionization potential and electron affinity, respectively, of the thin film. Furthermore, in deciding upon which voltage to pick as the ionization potential and electron affinity, the onset of current increase is taken instead of the peaks so as to indicate minimum values. The ionization energy can also be correlated to a highest occupied molecular orbital (HOMO) level, while the electron affinity can be correlated to a lower unoccupied molecular orbital (LUMO). A cyclic voltammogram of TBP is shown in Fig. 4. Scanning from 0 V to +2 V oxidizes the thin film, and resulting onset oxidation potential V_{ox} can be related to the ionization potential I_p by

$$I_p = q(V_{\text{ox}} - V_{\text{ref}}) + E_{\text{ref}} \quad (7)$$

where V_{ref} and E_{ref} are the voltage and corresponding energy at which the reference energy occurs. Conversely, by scanning from 0 to -3 V, the electrode bias reduces the thin film, and the resulting onset reduction potential V_{red} is related to the electron affinity E_a by

$$E_a = q(V_{\text{red}} - V_{\text{ref}}) + E_{\text{ref}}. \quad (8)$$

From Fig. 4, we deduce a $V_{\text{ox}} = 0.43$ V and a $V_{\text{red}} = -1.77$ V. In Fig. 4, the known energy level of ferrocene ($E_{\text{ref}} = 4.8$ eV) [20] occurs at an electrode voltage of 0.144 V. Therefore, the onset of the TBP ionization potential is 5.08 eV and the onset of the electron affinity is 2.89 eV. Here, we approximate the HOMO and LUMO levels by a conduction bandedge energy E_C and a valence bandedge energy E_V having a finite width. We take E_a and I_p as E_C and E_V , respectively. A transport bandgap

is also defined here as $E_T = E_C - E_V$, and is found to be about 2.2 eV. Values for the HOMO-LUMO levels of single-molecule forms of TBP range from 4.5–4.8 eV and 2.3–2.5 eV, respectively [33], [34]. Since many of the values reported in literature are for simulated or gaseous-phase single molecules, it is expected that they can differ from the values reported here.

Optical excitation of a thin film can provide information about the electronic states within a material. If an energy transition in the material is equal to that of the impinging photon energy, this wavelength is more strongly absorbed by the film as electrons are excited from a low energy state to a higher energy state. So in the presence of two energy levels E_2 and E_1 , the rate of absorbance will increase from zero for photons with an energy equal to the difference in the energies. Several types of transitions are important to consider when examining the absorption properties of a thin film. Band-to-band transitions occur when an absorbed photon excites an electron in the valence band into the conduction band, creating an electron-hole pair. Midgap-to-band transitions also manifest themselves when trap states are present within the bandgap. An absorbed photon can also excite an electron from the valence band into a trap level, from a trap level into the conduction band, or between trap levels. These types of transitions usually appear as an increased absorbance value at an energy lower than the bandgap. Furthermore, the rate of absorbance (photons per second per hertz per cubic centimeter) is directly related to the density-of-states at a photon frequency ν by [35], [36]

$$r_{ab}(\nu) = \phi_\nu \frac{\lambda^2}{8\pi\tau_r} \rho(\nu) f_a(\nu) \quad (9)$$

where ϕ_ν is the photon-flux spectral density, τ_r is the electron-hole recombination lifetime, $\rho(\nu)$ is the density-of-states, and $f_a(\nu)$ is the probability of absorption, which is dependent upon the filling of states in the valence and conduction bands. For c-Si, for example, $\rho(\nu)$ is given by an square root relation, while for a-Si:H $\rho(\nu)$ has a parabolic shape. Furthermore, when discussing the interband transitions of a semiconductor that might indicate the bandgap, the absorption (cm^{-1}) can be described by

$$\alpha(\nu) \approx \frac{\sqrt{2}c^2 m_r^{3/2}}{\tau_r (h\nu)^2} (h\nu - E_T)^{1/2} \quad (10)$$

where c is the speed of light, m_r is the reduced effective mass for holes and electrons, and h is Planck's constant. Therefore, plotting the absorbance on a linear scale versus photon energy reveals a bandedge where the absorbance curve intercepts the photon energy axis; this energy can be approximated as the bandgap of the semiconductor.

The optical absorbance spectrum of a TBP thin film is shown in Fig. 5. The maximum absorbance of the spectrum occurs at a photon energy of 2.77 eV, with an absorption edge at 2.3 eV ± 0.1 eV according to (10). This photon energy closely corresponds to E_T . Also prominent is an absorbance peak with a absorption edge around 1.7 eV ± 0.1 eV which could be associated with trap levels present within the gap of the semiconductor. The exact nature of such traps is under investigation. However, since TBP is a p-type organic semiconductor, the trap states are most

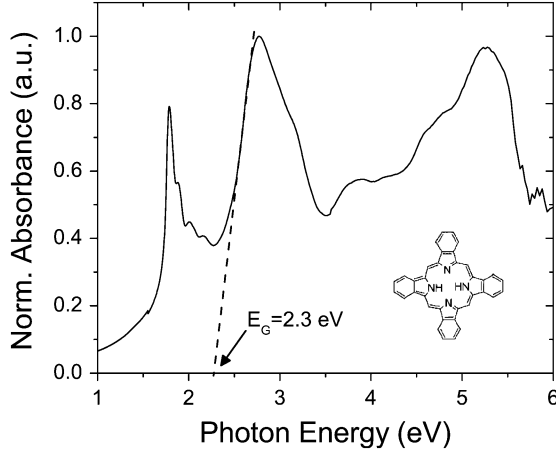


Fig. 5. Absorbance spectrum of a TBP thin film. The absorbance is normalized to the maximum between $1500 \geq \lambda(\text{nm}) \geq 200$, and is shown on a linear axis.

likely located closer to the valence band edge, e.g., $0.6 \text{ eV} \pm 0.1 \text{ eV}$ above E_V , while the 1.7-eV peak could correspond to a transition between the trap level and E_C . An alternative explanation could be that this absorbance energy is associated with a 1.7-eV exciton present in TBP. A higher energy photon-induced transitions above 4 eV, including a third peak at 5.3 eV, indicates that the polycrystalline TBP thin film have energy bands of nondiscrete levels above and below E_C and E_V ; the formation of such wide energy bands is also characteristic of polycrystalline materials.

V. ENERGY BAND DIAGRAMS

A combination of the electronic structure of TBP and the known workfunction of the Au source and drain electrodes ($q\phi_{\text{Au}} = 5.1 \text{ eV}$) [37], TBP OFET energy band diagrams can be drawn from the gate to the source electrode, and from the drain to the source electrode. In order to properly establish the effect of band-bending at the electrode-semiconductor interface, the Fermi energy level, E_F must first be found. We assume that for TBP, E_F is associated or controlled by the trap levels present in the thin film. We determined E_F by measuring the thermal activation energy, E_A , of the drain current in the device OFF-state and the ON-state. The OFF-state activation energy will correspond to the energy necessary to raise a charge carrier from the bulk Fermi level into the valence band edge; thus, the OFF-state E_A approximately equates to a bulk TBP Fermi level $E_{\text{FP-OFF}}$ of about $0.58 \text{ eV} \pm 0.1 \text{ eV}$; similar results were reported for the like molecule tetraphenylporphyrin [4]. The ON-state thermal activation energy corresponds to the accumulated channel energy $E_{\text{FP-ON}} = 0.25 \text{ eV}$ at $V_{\text{GS}} = -40 \text{ V}$.

In general, energy barriers to hole (ϕ_{Bp}) and electron injection (ϕ_{Bn}) for a p-type semiconductor can be given by

$$q\phi_{Bp} = E_C + E_T - q\phi_{\text{Au}} \quad (11a)$$

$$q\phi_{Bn} = q\phi_{\text{Au}} - E_C. \quad (11b)$$

When $E_T = 2.2 \text{ eV}$, we can calculate $q\phi_{Bp} = -0.01 \text{ eV}$ and $q\phi_{Bn} = 2.2 \text{ eV}$ for the Au-TBP interface. We can also define a built-in potential at the source and drain electrodes as

$$V_{bi} = q\phi_{\text{Au}} - q\phi_{Bp}. \quad (12)$$

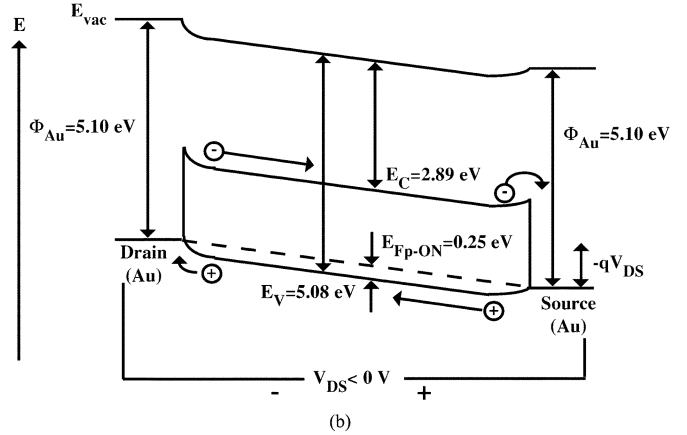
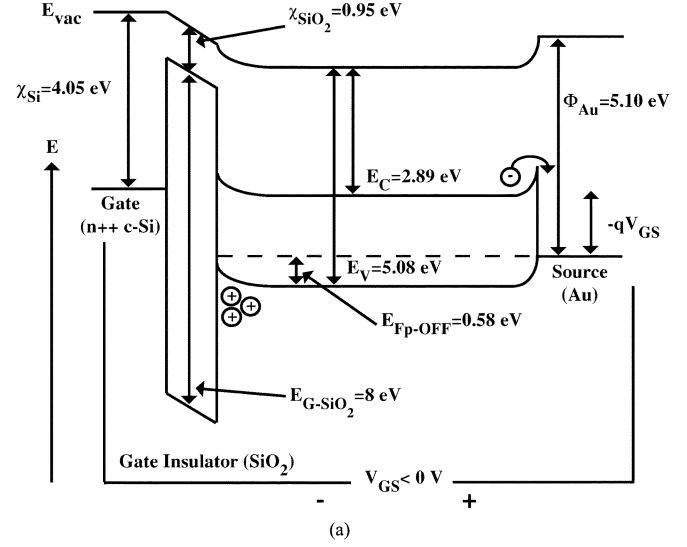


Fig. 6. Proposed energy band diagrams for a TBP OFET with Au S/D electrodes. (a) Gate to source. (b) Drain to source.

Therefore, in equilibrium, both the source and drain electrode see a $V_{bi} = 0.6 \text{ eV}$ to the bulk. Based on these values, the energy band diagrams for a TBP OFET were constructed and are displayed in Fig. 6. From gate-to-source in Fig. 6(a), holes are accumulated at the SiO_2 -TBP interface for a gate electrode biased negative in relation to the source. The ON-state activation energy, previously related to the Fermi level as $E_{\text{FP-ON}}$, gives the energy separation between the valence band edge and the Fermi level near the interface; $E_{\text{FP-OFF}}$ gives the energy separation in the bulk. Similarly, from drain-to-source in Fig. 6(b), holes in the channel travel from source-to-drain when the drain is biased negative in relation to the source. Holes can be created in the TBP channel when electrons are extracted at the source electrode. This hole then drifts toward the drain electrode, where it recombines with an electron injected from the drain. Furthermore, the bulk resistance that appears in staggered electrode devices [19] is not included in Fig. 6(b) as the ratio of the channel length ($L = 22.5 \mu\text{m}$) to the film thickness ($t_{\text{TBP}} = 120 \text{ nm}$) is very large.

To pinpoint the mechanism for charge conduction in TBP OFETs at low V_{DS} , temperature- and V_{GS} -dependent measurements were performed under low fields ($V_{\text{DS}} > -5 \text{ V}$). Given the linearity of the transfer characteristics [9], the conduction mechanism for a TBP OFET is likely confined to bulk and field-

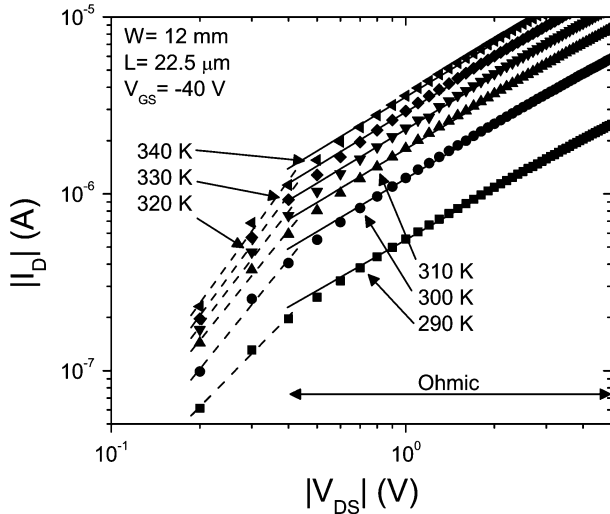


Fig. 7. Log-log plot of the TBP OFET low-electric-field output characteristics.

assisted tunneling mechanisms such as Poole-Frenkel emission [38], Fowler-Nordheim tunneling [21], and space-charge limited current (SCLC) [18] can be involved. In Fig. 7, for $V_{DS} > -0.4$ V either a Schottky barrier and/or SCLC limits the TBP OFET output characteristics. Since $q\phi_{Bp}$ is small, we can conclude that most likely SCLC is responsible for the nonlinearity mentioned above. In SCLC operation, the drain current can be described by

$$I_{DS} \propto V_{DS}^{\beta} \quad (13)$$

where β is the slope of the log-log curve. Two distinct regimes are visible in Fig. 7: a regime for $V_{DS} > -0.4$ V and a regime for $V_{DS} < -0.4$ V. For $V_{DS} < -0.4$ V, $\beta \approx 1$ and is independent of temperature and gate bias. Therefore, we can conclude that for $V_{DS} < -0.4$ V, the S/D contacts have no influence on the OFET characteristics. For $V_{DS} > -0.4$ V, $\beta > 1$ and is gate-bias- and temperature-dependent. In Fig. 8(a), β is seen to increase with both temperature and the gate bias. The temperature dependence can be described by

$$\beta = A - \frac{T_C}{T} \quad (14)$$

where T_C is the characteristic temperature of the trap states distribution in the material; A is a constant indicating the y axis intercept of the line, which in the ideal case equals 1. In Fig. 8(b), we show the fit of (14) to a plot of β versus $1/T$ for $V_{GS} = -40$ V. From this figure, we calculate $A = 5.53$ and $T_C = 1091.7$ K, which gives a trap energy of $kT_C = 0.094$ eV.

VI. CONCLUSION

We have examined the electrical properties of solution processable tetrabenzoporphyrin OFETs, with the source and drain electrodes fabricated in the staggered configuration. The output characteristics displays distinct linear and saturation regimes, while the transfer characteristics displays a high degree of linearity and a sharp subthreshold slope. A possible explanation for

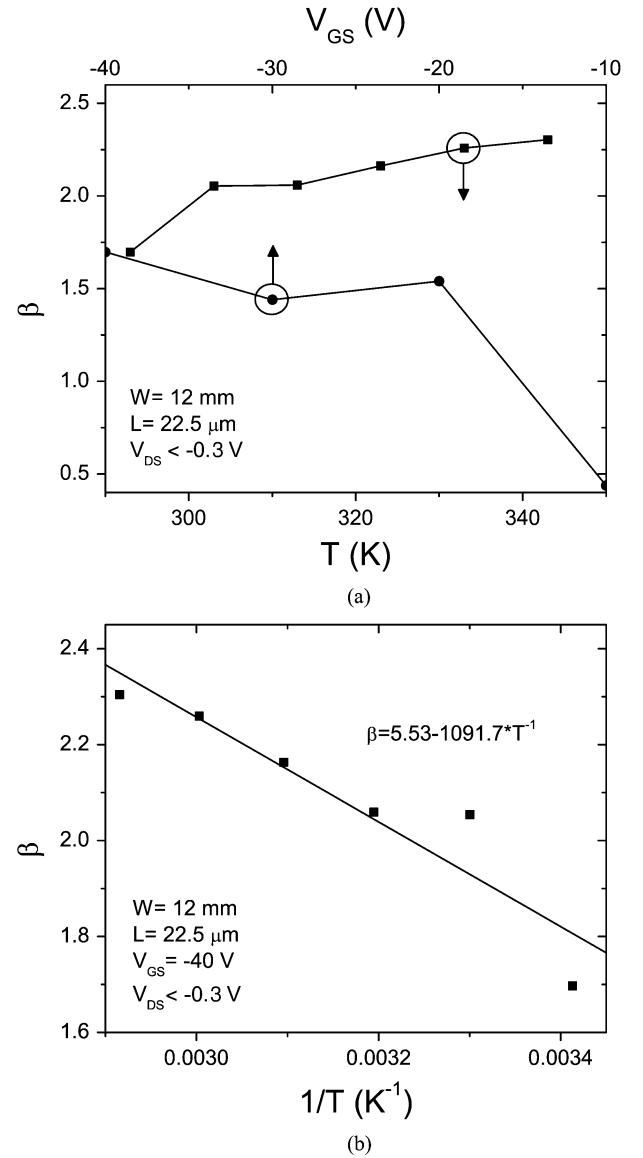


Fig. 8. Dependence of β with measurement temperature and gate bias.

such performance is sought in the electronic and optical properties of the TBP thin film. Cyclic voltammetry indicated the presence of the onset of the ionization potential near to the work-function of Au. Optical absorbance measurements indicated an optical gap with a value close to the transport gap measured with cyclic voltammetry, and also revealed the possible existence of trap states-based electronic transitions. All of these thin-film measurements were then combined to form energy band diagrams for a TBP OFET with Au S/D electrodes. A small degree of nonohmic behavior was observed for low drain bias, and was tested by varying the operating temperature and degree of channel accumulation.

REFERENCES

- [1] A. Brown, A. Pomp, D. de Leeuw, D. Klaassen, and E. Havinga, "Precursor route pentacene metal-insulator-semiconductor field-effect transistors," *J. Appl. Phys.*, vol. 79, pp. 2136–2138, 1996.
- [2] P. T. Herwig and K. Müllen, "A soluble pentacene precursor: Synthesis, solid-state conversion into pentacene and application in a field-effect transistor," *Adv. Mater.*, vol. 11, pp. 480–483, 1999.

- [3] A. Afzali, C. D. Dimitrakopoulos, and T. L. Breen, "High-performance, solution-processed organic thin film transistors from a novel pentacene precursor," *J. Amer. Chem. Soc.*, vol. 124, pp. 8812–8813, 2002.
- [4] P. Checcoli, G. Conte, S. Salvatoria, R. Paolesse, A. Bolognesi, M. Berliocchi, F. Brunetti, A. D'Amico, A. Di Carlo, and P. Lugli, "Tetra-phenyl porphyrin based thin film transistors," *Synth. Met.*, vol. 138, pp. 261–266, 2003.
- [5] M. Mushrush, A. Facchetti, M. Lefenfeld, H. Katz, and T. Marks, "Easily processable phenylene-thiophene-based organic field-effect transistors and solution-fabricated nonvolatile transistor memory elements," *J. Am. Chem. Soc.*, vol. 125, pp. 9414–9423, 2003.
- [6] S. Aramaki, Y. Sakai, and N. Ono, "Solution-processible organic semiconductor for transistor applications: Tetrabenzoporphyrin," *Appl. Phys. Lett.*, vol. 84, pp. 2085–2087, 2004.
- [7] F. Schreiber, "Organic molecular beam deposition: Growth studies beyond the first monolayer," *Phys. Stat. Sol. A*, vol. 201, pp. 1037–1054, 2004.
- [8] A. Brown, C. Jarrett, D. de Leeuw, and M. Matters, "Field-effect transistors made from solution-processed organic semiconductors," *Synth. Met.*, vol. 88, pp. 37–55, 1997.
- [9] P. B. Shea, J. Kanicki, and N. Ono, "Field-effect mobility of polycrystalline tetrabenzoporphyrin thin-film transistors," *J. Appl. Phys.*, 2004, submitted for publication.
- [10] C. D. Sheraw, T. N. Jackson, D. L. Eaton, and J. E. Anthony, "Functionalized pentacene active layer organic thin-film transistors," *Adv. Mater.*, vol. 15, pp. 2009–2011, 2003.
- [11] Y. Roichman and N. Tessler, "Two-dimensional simulation of polymer field-effect transistor," *Appl. Phys. Lett.*, vol. 79, pp. 2987–2989, 2001.
- [12] —, "Structures of polymer field-effect transistor: Experimental and numerical analyzes," *Appl. Phys. Lett.*, vol. 80, pp. 151–153, 2002.
- [13] R. Street and A. Salleo, "Contact effects in polymer transistors," *Appl. Phys. Lett.*, vol. 81, pp. 2887–2889, 2002.
- [14] M. Abkowitz, J. Facci, and J. Rehm, "Direct evaluation of contact injection efficiency into small molecule based transport layers: Influence of extrinsic factors," *J. Appl. Phys.*, vol. 83, pp. 2670–2676, 1998.
- [15] Y. Shen, M. W. Klein, D. B. Jacobs, J. C. Scott, and G. G. Malliaras, "Mobility-dependent charge injection into an organic semiconductor," *Phys. Rev. Lett.*, vol. 86, pp. 3867–3870, 2001.
- [16] J. C. Scott and G. G. Malliaras, "Charge injection and recombination at the metal-organic interface," *Chem. Phys. Lett.*, vol. 299, pp. 115–119, 1999.
- [17] L. Bürgi, T. Richards, R. Friend, and H. Sirringhaus, "Close look at charge carrier injection in polymer field-effect transistors," *J. Appl. Phys.*, vol. 93, pp. 6129–6138, 2003.
- [18] R. R. Troutman and A. Kotwal, "A device model for the amorphous-silicon staggered-electrode thin-film transistor," *IEEE Trans. Electron Devices*, vol. 36, no. 12, pp. 2915–2922, Dec. 1989.
- [19] J. Kanicki and S. Martin, "Hydrogenated amorphous silicon thin-film transistors," in *Thin-Film Transistors*, C. R. Kagan and P. Andry, Eds. New York: Marcel Dekker, 2003.
- [20] J. Pommerehne, H. Vestweber, W. Guss, R. Mahrt, H. Bassler, M. Porsch, and J. Daub, "Efficient 2-layer LED's on a polymer blend basis," *Adv. Mater.*, vol. 7, pp. 551–554, 1995.
- [21] S. M. Sze, *Physics of Semiconductor Devices*. New York: Wiley, 1981.
- [22] S. Martin, M. C. Hamilton, and J. Kanicki, "Source/drain contacts in organic polymer thin film transistors," in *Proc. Materials Research Society Symp.*, vol. 771, 2003, pp. 163–168.
- [23] M. Vissenberg and M. Matters, "Theory of the field-effect mobility in amorphous organic transistors," *Phys. Rev. B*, vol. 57, pp. 12964–12967, 1998.
- [24] G. Horowitz, R. Hajlaoui, H. Bouchriha, R. Bourguiga, and M. Hajlaoui, "The concept of threshold voltage in organic field-effect transistors," *Adv. Mater.*, vol. 10, pp. 923–927, 1998.
- [25] G. Horowitz, "Organic field-effect transistors," *Adv. Mater.*, vol. 10, pp. 365–377, 1998.
- [26] C. Dimitrakopoulos and D. Mastro, "Organic thin-film transistors: A review of recent advances," *IBM J. Res. Dev.*, vol. 45, pp. 11–27, 2001.
- [27] S. Scheinert and G. Paasch, "Fabrication and analysis of polymer field-effect transistors," *Phys. Stat. Sol. A*, vol. 201, pp. 1263–1301, 2004.
- [28] A. Rolland, J. Richard, J. P. Kleider, and D. Mencaraglia, "Electrical properties of amorphous silicon transistors and MIS-devices—Comparative study of top nitride and bottom nitride configurations," *J. Electrochem. Soc.*, vol. 140, pp. 3679–3683, 1993.
- [29] G. Horowitz, "Tunneling current in polycrystalline organic thin-film transistors," *Adv. Funct. Mater.*, vol. 13, pp. 53–60, 2003.
- [30] M. C. Hamilton, S. Martin, and J. Kanicki, "Field-effect mobility of organic polymer thin-film transistors," *Chem. Mater.*, vol. 16, pp. 4699–4704, 2004.
- [31] J. F. Rusling and S. L. Suib, "Characterizing materials with cyclic voltammetry," *Adv. Mater.*, vol. 6, pp. 922–930, 1994.
- [32] S. Janietz, D. Bradley, M. Grell, and C. Giebler, "Electrochemical determination of the ionization potential and electron affinity of poly(9,9-dioctylfluorene)," *Appl. Phys. Lett.*, vol. 73, pp. 2453–2455, 1998.
- [33] L. K. Lee, N. H. Sabelli, and P. LeBreton, "Theoretical characterization of phthalocyanine, tetraazaporphyrin, tetrabenzoporphyrin, and porphyrin electronic spectra," *J. Phys. Chem.*, vol. 86, pp. 3926–3931, 1982.
- [34] X. Zhou, A. Ren, J. Feng, and X. Liu, "Theoretical studies on the one- and two-photon absorption of tetrabenzoporphyrins and phthalocyanines," *Can. J. Chem.*, vol. 82, pp. 19–26, 2004.
- [35] B. Saleh and M. Teich, *Fundamentals of Photonics*, 1st ed. New York: Wiley-Interscience, 1991.
- [36] P. K. Bhattacharya, *Semiconductor Optoelectronic Devices*, 2nd ed. Englewood Cliffs, NJ: Prentice-Hall, 1997.
- [37] [Online]. Available: <http://www.environmentalchemistry.com/yogi/periodic>
- [38] J. Frenkel, "On pre-breakdown phenomena in insulators and electronic semiconductors," *Phys. Rev.*, vol. 54, pp. 647–648, 1938.



Patrick B. Shea (S'03) received the B.S. degree in electrical engineering from the University of Notre Dame, Notre Dame, IN, in 2002, and the M.S. degree in electrical engineering from the University of Michigan, Ann Arbor, in 2003. He is currently pursuing the Ph.D. degree in electrical engineering at the University of Michigan.

He joined the Organic and Molecular Electronics Laboratory, Solid State Electronics Laboratory, Department of Electrical Engineering and Computer Science (EECS), University of Michigan, in 2003.

His research interests include organic semiconductor physics and optoelectronic devices.



Aaron R. Johnson received the B.S. degree in physics, the B.E.E. degree in electrical engineering, and the B.A. degree in philosophy from the University of Louisville, Louisville, KY, in 2001. He is currently enrolled in the Macromolecular Science and Engineering program at the University of Michigan in the Organic and Molecular Electronics Laboratory.

His research involves top-emitting OLEDs and alternative OLED architecture.

Noboru Ono received the Ph.D. degree in chemistry from the Faculty of Science, Kyoto University, Kyoto, Japan, in 1970.

From 1973 to 1986, he was a member of the Chemistry Department at Kyoto University. Since 1990, he has been a Professor of Chemistry at Ehime University, Ehime, Japan. His research interests focus on the development of novel synthesis methods for organic molecules, including porphyrins and phthalocyanines.



Jerzy Kanicki (M'99–A'99–SM'00) received the Ph.D. degree in sciences (D.Sc.) from the Université Libre de Bruxelles, Brussels, Belgium, in 1982.

He subsequently joined the IBM Thomas J. Watson Research Center, Yorktown Heights, NY, as a Research Staff Member, working on hydrogenated amorphous silicon devices for photovoltaic and flat-panel display applications. In 1994, he moved from IBM Research Division to the University of Michigan, Ann Arbor, as a Professor in the Department of Electrical Engineering and Computer

Science (EECS). His research interests within the Electrical and Computer Engineering division of EECS include organic and molecular electronics, TFTs and circuits, and flat-panel displays technology, including organic light-emitting devices.